BioNanoScience (2024) 14:3226–3240
https://doi.org/10.1007/s12668-024-01417-w

RESEARCH

Irreversibility Processes on the Squeezing Flow Analysis of Blood-Based Micropolar Hybrid Nanofluid Through Parallel Channel: Spectral Quasilinearisation Method

Titilayo M. Agbaje[1] · Rupa Baithalu[2] · S. R. Mishra[2] · Subhajit Panda[3]

Accepted: 21 April 2024 / Published online: 3 May 2024
© The Author(s), under exclusive licence to Springer Science+Business Media, LLC, part of Springer Nature 2024

Abstract
The biomedical applications along with nanotechnology field have generated considerable interest because of their unique thermal properties. The present investigation explores the irreversibility processes for the squeezing flow of a polar hybrid nanofluid where blood is considered the conventional liquid and copper (*Cu*) and Silver (*Ag*) are introduced as solid nanoparticles. The integration of dissipative heat effects (viscous and Joule) combined with thermal radiation adequately enhances the transport phenomena. Furthermore, the unique rheological significance of blood-based nanofluids is relevant for efficient drug delivery systems, improving circulation, optimizing side effects, etc. The essential study of entropy is used for optimizing the design and efficiency of devices used in various tasks ranging from medical diagnostics to environmental monitoring. The proposed system of dimensional equations is diverting into non-dimensional system by the use of similarity rules, and further, the spectral quasilinearization method is employed to tackle the transformed system. The parametric analysis upon the various flow profiles, rate coefficients, and entropy as well as the Bejan number is depicted through graphs, and the validation shows a good correlation in a particular situation.

Keywords Blood-based Hybrid Nanofluid · Joule Dissipation · Thermal Radiation · Channel Flow · Entropy Analysis · Spectral Quasilinearization Method

1 Introduction

A micropolar hybrid nanofluid is a complex fluid system that combines the characteristics of micropolar fluids and nanofluids. Micropolar fluids exhibit unique properties due to the consideration of micro-rotations within the fluid structure. Hybrid nanofluids, on the other hand, involve the diffusion of nanocomposites in a conventional liquid. The combination of these features in a micropolar hybrid nanofluid introduces novel rheological and thermal properties, making it a subject of interest in various scientific and engineering applications, including heat transfer enhancement and biomedical fluid dynamics. In particular, blood-based nanofluids play a crucial role in designing drug delivery system. It aims to transport drug to specific target sites while minimizing side effects. However, blood circulation is important for delivering oxygen and nutrients throughout the body. The physical properties of blood enhance the flow dynamics. By controlling the rheological properties of the nanofluid and the characteristics of the drug carrier, it enhances drug accumulation at the target site. This targeted delivery approach mitigates side effects associated with off-target drug distribution. The slippery motion of a Casson nanofluid over a non-linear widening sheet was explored by Sarwar et al. [1], considering the significant association of an inclined magnetized field together with radiative heat flux. Utilizing the shooting

✉ Rupa Baithalu
rupadhananjaygarnaik@gmail.com

Titilayo M. Agbaje
titilayoagbaje@gmail.com

S. R. Mishra
satyaranjan_mshr@yahoo.co.in

Subhajit Panda
spanda.math@gmail.com

[1] School of Computer Science and Applied Mathematics, University of the Witwatersrand, Johannesburg, South Africa

[2] Department of Mathematics, Siksha 'O' Anusandhan Deemed to Be University, Bhubaneswar, Odisha 751030, India

[3] Centre for Data Science, Siksha 'O' Anusandhan Deemed to Be University, Bhubaneswar, Odisha 751030, India

scheme in coincidence with Runge–Kutta, numerical solutions are acquired for the given boundary values problem. An inclined magnetic field finds diverse applications in science and technology, spanning areas such as magnetic resonance imaging (MRI), particle accelerators, magnetic levitation (Maglev), magnetic recording technologies, magnetometers, and compasses. This orientation of the magnetic field serves pivotal roles across various technological and scientific domains. In their observation, Lone et al. [2] investigated the influence of bioconvective motion in Casson nanofluids. The research involved employing a base liquid to simulate blood, with the addition of magnesium nanoparticles into the host fluid to form an effective nanofluid blend. In the study conducted by Baithalu et al. [3], an investigation was carried out on the motion of a magnetopolar-hybridized nanofluid over an elastic surface. The study emphasized the significance of both shear rate and couple stresses in influencing the flow behavior. The nanofluid, immersed with Ag and MoS4 nanoparticles in a base fluid of water, was examined to understand their impact on the overall flow characteristics. Their work utilized the *response surface methodology* (RSM) along with *analysis of variance* (ANOVA) to optimize key parameters, contributing to a comprehensive analysis of the fluid flow dynamics. Farooq et al. [4] investigated the motion of fluid flow and thermal transportation of Casson nanofluid along a cylinder/plate in two dimensions, exploring the mutual impacts of thermophoresis along with Brownian motion in their study. Furthermore, the resulting set of non-linear ordinary differential equations solved numerical evaluation using the bvp4c within the MATLAB mathematical solver. In their study, Mishra et al. [5] examined how particle shape influences the radiative motion of a Casson-hybridized nanoliquid toward an elastic or diminishing convective sheet. Furthermore, the hybrid nanofluid discussed in this investigation consists of water and carbon nanotubes (CNTs) with varying particle shapes. A Casson-type model is utilized to determine the nanofluid's rheological property while accounting for the fluid's non-Newtonian dynamics. Panda et al. [6] presented the Williamson fluid flowing through two inclined parallel sheets. Additionally, the significant association of thermal radiation and Ohmic heating is discussed. Moreover, the *homotopy perturbation method (HPM*) is implemented analytically to the finalized transformed equations. Shao et al. [7] investigated the optimization of thermal transmission rates in a squeezing channel featuring micropolar nanofluid flow, employing advanced statistical concepts. Their study assessed the influence of diverse constraints on heat transfer performance through response surface methodology (RSM).

Magnetic resonance imaging (MRI), particle accelerators, magnetic levitation (Maglev), magnetic recording technologies, magnetometers, and compasses are just a few of the many scientific and technological uses for magnetic fields. This magnetic field orientation plays important roles in many scientific and technological fields. The magnetic nanofluid, which is a cutting-edge nanotechnology application, consists of nanoscale magnetic particles suspended in a fluid medium. These unique fluids exhibit remarkable properties such as enhanced thermal conductivity and tunable magnetization. The magnetic nanoparticles within the fluid can be manipulated using external magnetic fields, making them promising for various applications, including targeted drug delivery and advanced cooling systems. This liquid flow entails a hybridized nanofluid immersing Fe3O4 and CoFe2O4 nanoparticles dispersed in water, through a diminishing Riga surface with velocity slip constraints. Panda et al. [8] considered the integration of significant conductivity models like the Hamilton-Crosser and Yamada-Ota models. The resolution of governing equations involved a collaborative application of the *Runge–Kutta-Fehlberg (RKF) method* and the shooting scheme. Azam et al. [9] studied the intricate dynamics of transient bioconvection flow over an expanding/contracting cylinder, with a focus on the influence of cross nanofluid. Bioconvection phenomena, characterized by the collective motion of microorganisms, take center stage in this investigation, shedding light on its influence on the liquid flow. Additionally, the model takes into account the significant contribution of nonlinear radiation, highlighting its role in shaping the thermal behavior of the system. Khan et al. [10] explored the utilization of viscoelastic nanoparticles in conjunction with mobile microorganisms within a wedge-shaped geometry. Furthermore, the analysis is conducted within the context of the melting process, offering insights into the complex interplay of these factors in this specific geometric configuration. Habib et al. [11] recently conducted a comparative analysis of mass and thermal transport outcomes within different fluid models, together with various Newtonian and non-Newtonian fluids under the influence of an elastic surface. Their work developments specifically evaluate the impact of double diffusion and the application of a magnetic field. Waqas et al. [12] explored the behavior of Sutterby nanofluid subjected to an applied magnetic field and convective boundary elements, utilizing two coaxially rotating stretching discs. Nanofluids, comprised of simple fluids with evenly distributed small particles in the base fluid, hold promising prospects for thermal transport applications. They enhance heat transfer coefficients by incorporating nanomaterials into the base fluids. This investigation specifically targets non-Newtonian base fluids, employing the Sutterby model. Ordinary differential equations (ODEs) are addressed through shooting techniques, and the results of key physical parameters are obtained using the bvp4c solver in MATLAB computational software. The present study centers on examining the interaction among magnetic dissipation, as well as inertial drag within an expanding permeable medium, as explored by Nayak et al. [13]. Their work's significance lies in the simultaneous impact of a uniform magnetic

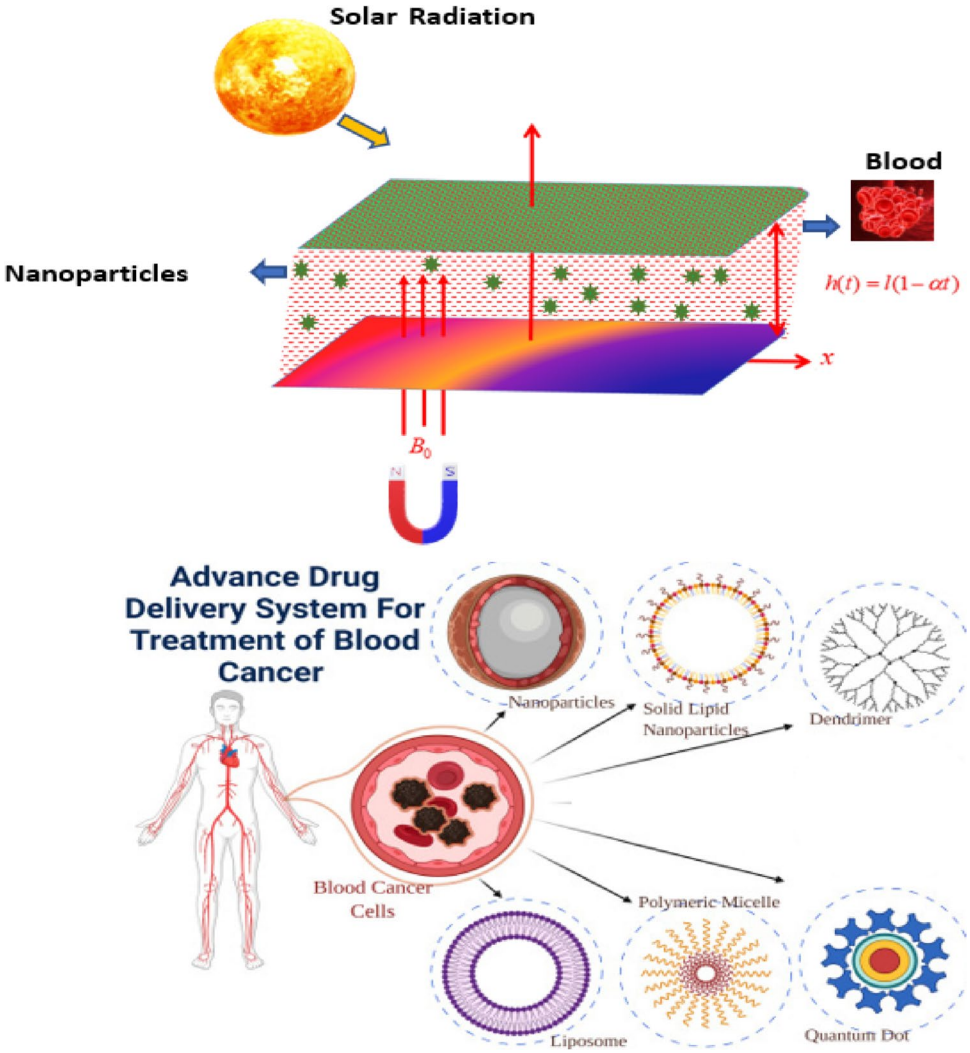

Fig. 1 Flow geometry

field and an electric field. The mathematical model, employing the Buongiorno nanofluid model, is intricately designed, and the resulting set of ordinary equations is transformed using a suitable similarity transformation. Lone et al. [14] examined the mutual association of dissipation on thermal energy as well as inertial drag in the context of free convective flow over an expanding permeable medium. The unique aspect of this study is the investigation of the collective influence of a uniform magnetic field and an electric field. Developing a mathematical model in alignment with the Buongiorno nanofluid model, the set of equations is transformed using suitable similarity transformations. To numerically solve these equations, the traditional shooting-based Runge–Kutta fourth-order technique is employed. Saleem et al. [15] examined the insertion of radiative heat flux as well as magnetized Casson nanofluid motion along a nonlinear widening surface. The analysis considers simultaneous incorporation of suction and a homogeneous magnetic field. The article introduces an efficient *Levenberg–Marquardt methodology* for *artificial neural networks* (ANNs), a back-propagation algorithm with minimal nonlinear latency. Raut et al. [16] examined the varied influence of carbon nanotubes (CNTs) on micropolar nanofluid flow considering a porous widening/diminishing surface embedded in a permeable medium. Additionally, the governing nonlinear partial differential equations are transformed into a set of nonlinear ordinary differential equations using appropriate similarity conversion rules. Subsequently, these equations are numerically solved using the fourth-order Runge–Kutta technique based on the shooting method. Hayat et al. [17] investigated the stream of a viscous fluid adjacent to a revolving disk. Their study disregards heat generation and absorption, employing an entropy generation analysis based on the second law of thermodynamics. Iqbal et al. [18] examined the Eyring–Powell nanofluid under the addition of Cattaneo–Christov heat flux and gyrotactic microorganisms' motion in the presence of a strong magnetic field. The *homotopy analysis method (HAM)* is used to solve the nonlinear ordinary differential equations. The association of various factors is analyzed in detail. Mukdasai et al. [19] explored a numerical analysis of double diffusion as well as gyrotactic microorganisms in a complex fluid, specifically over a widening cylinder

and surface. In their work, Fatima et al. [20] deliberated a numerical investigation into the boundary layer motion through a mobile horizontal flat plate immersed with nanofluid. The study included variable temperatures at the wall and accounted for viscous dissipation in the presence of gyrotactic microorganisms. The transformed ordinary differential equations were subsequently solved using the MATLAB built-in bvp4c scheme. Yusuf's [21, 22] investigation focuses on thermodynamic analysis and entropy generation analysis which affects the dynamics of unsteady nanofluid flow and heat transfer along a vertical plate; the altered equations are numerically integrated using the "spectral quasilinearization approach." Finally, an average entropy generation retards with the inclusion of a temperature- and space-dependent heat source/sink, while an enhancement in the viscosity parameter leads to improvement. Additionally, the entropy generation rate is enhanced with variations in the Reynolds number and volume fraction parameter. Yusuf et al. [23] investigated the semi-analytical solution concerning the rate of entropy generation in a steady flow of a micropolar fluid, driven by gravity, cascading over a heated inclined substrate while adhering to slip constraints. Employing a comprehensive semi-analytical methodology, specifically the *differential transformation method*, was pivotal in deriving the solution for the nonlinear governing model. The findings of this research reveal that an increase in the micro rotation parameter values leads to a decrease in the velocity gradient while simultaneously enhancing thermal effects, dimensionless Bejan number, and entropy generation profiles along the incline. Yusuf et al. [24, 25] examined the impact of thermal radiation on the magnetohydrodynamic flow of a Williamson nanofluid and slip effect and evaluated entropy production in hybrid nanofluids over a stretching sheet with chemical reaction as well as porous medium. A distinctive aspect of this study lies in its focus on thermodynamic analysis within the nonlinear convective flow of a Williamson nanofluid. Furthermore, slip flow is incorporated into a Darcy-Forchheimer model, along with nonlinear thermal radiation effects. Water serves as the base fluid, with the inclusion of copper and titanium dioxide nanoparticles. Finally, the study investigates the influence of relevant parameters on flow characteristics, heat transfer, and rates of entropy generation. Khan et al. [26] explored the flow of magnetized water-based carbon nanotubes also examining chemical reactive flow within a Darcy-Forchheimer porous space. Moreover, a model is developed for the relation between volumetric entropy generation rates. Finally, numeric solutions are obtained using a shooting scheme approach. Ahmed et al. [27, 28] investigated the solutions obtained for the square lid-driven cavity that describe classical mixed convection in the presence of heat generation, chemical radiation, and an inclined magnetic field as well as the homogeneous heterogeneous reactions in the magnetohydrodynamic boundary layer stalled flow of an Al2O3-Cu-water base hybrid nanofluid past a stretched decreasing sheet. Mathematically, the problem is reduced to Navier–Stokes equations. These nonlinear partial differential equations with their non-homogeneous boundary conditions are then solved using a recently proposed computing method called the *Coiflet wavelet homotopy approach*. Furthermore, the results show that their currently proposed approach has superior characteristics and strong nonlinear processing capabilities, making it more suitable for dealing with complex nonlinear problems than the Coiflet wavelet analysis method and the traditional "homotopy analysis method." A new hybrid nanofluid model is crafted by Ahmed et al. [29] for integrating key slip mechanisms such as Brownian diffusion and thermophoresis. To validate this innovative model, the study investigates the flow and heat transfer characteristics within a lid-driven square cavity filled with a porous medium. Employing the "Coiflet wavelet homotopy analysis method," numerical findings are presented, focusing on Brownian motion and thermophoresis effects. Ahmed et al. [30] examined the natural convection of a complex fluid comprising nanoparticles and gyrotactic microorganisms within a heated square cavity. Furthermore, they utilize the *Buongiorno model* to characterize the nanofluid dynamics. The non-dimensional governing equations are derived using the stream-vorticity formulation and solved using the *robust Coiflet wavelet homotopy analysis method*, which has been recently developed. Ahmed et al. [31] investigated the dynamics of a hybrid nanofluid flowing through a microchannel under the influence of a time-dependent periodic pressure gradient. Furthermore, their work incorporates the presence of an electric double layer, magnetic field, and thermal radiation effects. Moreover, electrostatic potential is modeled using the Boltzmann-Poisson equation, while the conservation of momentum and thermal energy is described by employing the reduced Navier–Stokes equations, assuming small pressure amplitudes.

1.1 The Prime Objectives

The main focus point of the proposed investigation is to explore the irreversibility processes due to various properties like heat transfer, diffusion, and dissipation occurring in the squeezing flow of a blood-based micropolar hybrid nanofluid through a parallel channel. In particular, the aim is to explore the role of these irreversibility processes on the flow behavior, providing the efficiency and potential challenges relating to the drug delivery processes utilizing such nanofluid systems.

1.2 Novelty of the Proposed Model

The novelty of this study lies in several aspects:

- The utilization of microscale polar particles in a hybrid nanofluid, combined with biological fluid blood as the base fluid, presents a novel approach.

- The thermophysical properties to the hybrid nanofluid, making it suitable for biomedical applications like drug delivery.
- Squeezing flows are pertinent in various biological and medical contexts, including microfluidic devices and physiological processes for optimizing drug delivery mechanisms.
- The analysis on the irreversibility processes within the squeezing flow plays a significant role in determining the efficiency and energy dissipation characteristics of fluid flows.
- The application of the spectral quasilinearization method for analyzing the squeezing flow of the hybrid nanofluid introduces a novel computational technique.

1.3 Limitations of the Study

Based upon the objective and novelty of the study, the innovative approach to utilizing hybrid nanofluid for biomedical applications has certain limitations.

- The current investigation lacks experimental validation of the results obtained, while theoretical analyses and mathematical modeling are important.
- The compatibility of the hybrid nanofluids which has biomedical applications like drug delivery needs thorough investigation.
- The long-term stability of the hybrid nanofluids in biological environments is uncertain.

2 Description of Current Model

The problem of two plates at a distance $h(t) = l\sqrt{(1-\alpha t)}$. The upper plate makes contact with the lower plate at $t = 1/\alpha$ while moving at a velocity dh/dt considering the blood as the base fluid in a micropolar nanofluid flow between two parallel plates. Vertical and horizontal alignment exists between the x- and y-axes. Assuming constant temperature H_1 at the upper plate, at the center of the channel it has no heat flux. The horizontal plates' direction is affected by the magnetic flux (Fig 1).

The flow and energy equations can be expressed as follows (Mustafa [32]):

$$\partial_x u + \partial_y v = 0 \tag{1}$$

$$\rho_{nf}[\partial_t u + u\partial_x u + v\partial_y u] = -\partial_x P + (\mu_{nf} + k)(\partial_{xx}u + \partial_{yy}u) + k\partial_y N - \sigma_{nf}B_0^2 u - \mu_{nf}K^{*-1}u \tag{2}$$

$$\rho_{nf}[\partial_t u + u\partial_x v + v\partial_y v] = -\partial_y P + (\mu_{nf} + k)(\partial_{xx}v + \partial_{yy}v) - k\partial_x N - \sigma_{nf}B_0^2 v - \mu_{nf}K^{*-1}v \tag{3}$$

$$\rho_{nf}[\partial_t N + u\partial_x N + v\partial_y N] = -2kN + k(\partial_x v + \partial_y u) + (\mu_{nf} + k/2)j(\partial_{xx}N + \partial_{yy}N) \tag{4}$$

$$(\rho c)_{nf}[\partial_t T + u\partial_x T + v\partial_y T] = (k_{nf} + 16/3k^{*-1}\sigma^* T_1^3)(\partial_{xx}T + \partial_{yy}T)(\mu_{nf} + k/2)j((\partial_x N)^2 + (\partial_y N)^2) + k/2(\partial_x v - \partial_y u - 2N)^2 + 4\mu_{nf}(\partial_y v)^2 + \mu_{nf}(\partial_y u + \partial_x v)^2 + \sigma_{nf}B_0^2(u^2 + v^2) \tag{5}$$

where (u, v) are the velocities along (x, y) direction.

The models against the thermophysical properties of nanofluid are assumed as follows:

Viscosity: $\mu_{nf} = \mu_f(1 + 2.5\phi + 6.25\phi^2)$ (Brinkman model).

Density: $(\rho)_{nf} = (1-\phi)\rho_f + \phi(\rho)_s$ (Maxwell model).

Specific heat: $(\rho c)_{nf} = (1-\phi)(\rho c)_f + \phi(\rho c)_s$ (Maxwell model).

Thermal conductivity: $\frac{k_{nf}}{k_f} = \frac{k_s+(n-1)k_f-(n-1)\phi(k_f-k_s)}{k_s+(n-1)k_f+\phi(k_f-k_s)}$ (Hamilton-Crosser model).

Electrical conductivity: $\frac{\sigma_{nf}}{\sigma_f} = 1 + \frac{3(\sigma-1)\phi}{\sigma+2-(\sigma-1)\phi} and \sigma = \frac{\sigma_s}{\sigma_f}$ (Maxwell model).

The proposed surface conditions are as follows (Mustafa [32]):

$$\left.\begin{array}{c} N = 0, \partial_y u = 0, v = 0, \partial_y T = 0, aty = 0 \\ N = 0, u = 0, v = v_w, T = T_1, aty = h \end{array}\right\} \tag{6}$$

Following Mustafa [32], the similarity transformations are

$$\left.\begin{array}{c} \eta = \frac{y}{l\sqrt{(1-\alpha t)}}, N = \frac{\alpha x}{2l(1-\alpha t)^{3/2}}g(\eta), \\ v = \frac{-\alpha l}{2\sqrt{(1-\alpha t)}}f(\eta), u = \frac{-\alpha x}{2(1-\alpha t)}f'(\eta), \theta = \frac{T}{T_1} \end{array}\right\} \tag{7}$$

Substituting the transformation in the governing equation, there is a set of coupled non-linear ordinary differential equations and these are presented.

$$\left.\begin{array}{c} L_f(f,g,\theta) = (A_1 + K)f^{iv} + Kg'' - MA_3 f'' - DaA_1 f'' - SqA_2 f''' \\ N_f(f,g,\theta) = -SqA_2(3f'' + f'f'' - f'f''') \end{array}\right\} \tag{8}$$

$$\left.\begin{array}{c} L_g(f,g,\theta) = S_1(A_1 + \frac{K}{2})g'' - Kf'' - 2Kg - A_2 SqS_1(3g + \eta g') \\ N_g(f,g,\theta) = -A_2 SqS_1(f'g - fg') \end{array}\right\} \tag{9}$$

$$\left.\begin{array}{c} L_\theta(f,g,\theta) = (A_4 + Nr)\theta'' - A_5 Sq\Pr\eta\theta' \\ N_\theta(f,g,\theta) = A_5 Sq\Pr f\theta' + \frac{K\Pr Ec}{2}\left(f'' + 2g\right)^2 + \frac{\Pr Ec}{A_1}\left(4f'^2\delta^2 + f''^2\right) \\ \frac{\Pr EcS_1}{A_1}[1 + \frac{K}{2}(1-\phi)^{2.5}](\delta^2 g^2 + g'^2) + \Pr EcMA_3(\delta^2 f^2 + f'^2) \end{array}\right\} \tag{10}$$

where $Nr = \frac{16\sigma T_1^3}{3k^* k_f}$, $Ec = \frac{\alpha^2 x^2}{4cp_f T_1(1-\alpha t)^2}$, $M = \frac{\sigma B_0^2 l^2}{\mu}$, and $K = \frac{k}{\mu_f}$ are the non-dimensional vortex viscosity parameters, and $\delta = \frac{l\sqrt{(1-\alpha t)}}{x}$ is a non-dimensional micropolar parameter. $S_1 = \frac{x_j}{l^2(1-\alpha t)}$ is the micropolar parameter, and $S_q = \frac{\alpha l^2}{2\upsilon}$ is the

squeezing parameter. The other nanoparticles' volume fraction-dependent parameters are written as

$$\left.\begin{aligned} A_1 = 1 + 2.5\phi + 6.25\phi^2, A_2 = (1-\phi) + \phi\frac{\rho_s}{\rho_f}, A_3 = 1 + \frac{3(\sigma-1)\phi}{\sigma+2-(\sigma-1)\phi}, \\ A_4 = \frac{k_s+(n-1)k_f-(n-1)\phi(k_f-k_s)}{k_s+(n-1)k_f+\phi(k_f-k_s)}, A_5 = (1-\phi) + \phi\frac{(\rho c)_s}{(\rho c)_f} \end{aligned}\right\} \tag{11}$$

The values for $A_1, A_2, A_3, A_4 and A_5$ are designed for the assumed thermophysical models described earlier.

Again, the substitution of similarity transformations Eq. (12) into Eq. (11) results to the following dimensionless boundary conditions:

$$\left.\begin{aligned} g(0) = 0, f''(0) = 0, f(0) = 0, \theta'(0) = 0, \\ g(1) = 0, f'(1) = 0, f(1) = 1, \theta(1) = 1, \end{aligned}\right\} \tag{12}$$

The dimensionless viscous drag at $\eta = \pm 1$ is

$$C_f = \frac{2\tau}{\rho v_w^2} = -(A_1 + K)f''(\eta) \tag{13}$$

The dimensionless couple stress at $\eta = \pm 1$ is

$$C_s = -g'(\eta) \tag{14}$$

The Nusselt number at $\eta = \pm 1$ is

$$Nu = -(A_4 + Nr)\theta'(\eta) \tag{15}$$

The Sherwood number at $\eta = \pm 1$ is

$$Sh_x = -\omega'(\eta) \tag{16}$$

3 Entropy Generation

Entropy generation is a general concept in thermodynamics to quantify the irreversibility of processes. This process is due to frictional heating, heat transfer, dissociative heat effect, etc. Entropy generation is calculated by using the entropy balance equation, which accounts for entropy generation within control volume because of heat transfer, fluid flow, and the irreversibility defined earlier. Though higher entropy generation corresponds to lower efficiency, it has implications for the efficiency of energy conservation. The total entropy is defined as

$$E_G = \frac{k_f}{H_1^2}\left(\frac{k_{nf}}{k_f} + \frac{16\sigma^* T_1^3}{3k^* k_f}\right)[(\partial_x T)^2 + (\partial_y T)^2] + \frac{1}{T_1}(\mu_{nf} + \frac{k}{2})j[(\partial_x N)^2 + (\partial_y N)^2] + \frac{k_1}{2T_1}(\partial_x v + \partial_y u - 2N)^2 + \frac{4\mu_{nf}}{T_1}(\partial_x u + \partial_y v)^2 + \frac{\mu_{nf}}{T_1}(\partial_y u + \partial_x v)^2 + \frac{\sigma_{nf}B_0^2}{T_1}(u^2 + v^2) \tag{17}$$

And the Bejan number, a dimensionless parameter in thermodynamics is used to characterize the relative importance of entropy generation and heat transfer within a system. It is defined as the ratio of entropy generation due to heat transfer and total entropy.

$$Be = \frac{k_f}{S_G T_1^2}\left(\frac{k_{nf}}{k_f} + \frac{16\sigma^* T_1^3}{3k^* k_f}\right)[(\partial_x T)^2 + (\partial_x T)^2] \tag{18}$$

In the non-dimensional form, it may be written as

$$E_G^* = (A_4 + Nr)\theta'^2 + Br_1\left(1 + \frac{K(1-\phi)^{2.5}}{2}\right)\left(g^2 + \delta^2 g'^2\right) + Br_2(f''' + \frac{Br_3}{(1-\phi)^{2.5}}(\frac{\delta^2 f''^2}{4} + f'^2) + \frac{A_3 MBr_3}{4}(f^2 + \delta^2 f'^2) \tag{19}$$

$$Be = \frac{(A_4 + Nr)\theta'^2}{E_G^*} \tag{20}$$

where

$$Br_1 = \frac{\mu_f j\alpha^2}{4k_f T_1(1-\alpha t)^2}, Br_2 = \frac{\mu_f x^2\alpha^2}{8k_f T_1(1-\alpha t)^2}, Br_3 = \frac{\mu_f l^2\alpha^2}{k_f T_1(1-\alpha t)^2}$$

4 Method of Solution

The ordinary differential equations (ODEs) derived, along with their corresponding boundary conditions governing both flow and heat transport, are rendered non-dimensional by introducing appropriate variables. To solve these non-dimensional ODEs, the spectral quasilinearization method (SQLM) is employed. The SQLM utilized in this investigation combines the Newton–Raphson-based linearization technique (QLM) with the Chebyshev spectral method. This method entails linearizing the governing equations through a Taylor series expansion, assuming small differences between the values of the unknown function at current $(s+1)$ and previous (s) iteration levels. For a more comprehensive understanding of the SQLM, please refer to [33]. Applying the QLM to the derived ODEs, using a one-term Taylor series expansion for multiple variables yields

$$a_{0,s}f''''_{s+1} + a_{1,s}f'''_{s+1} + a_{2,s}f''_{s+1} + a_{3,s}f'_{s+1} + a_{4,s}g''_{s+1} = RHS1, \tag{21}$$

$$b_{0,s}g''_{s+1} + b_{1,s}g'_{s+1} + b_{2,s}g_{s+1} + b_{3,s}f''_{s+1} + b_{4,s}f'_{s+1} + b_{5,s}f_{s+1} = RHS2, \tag{22}$$

$$c_{0,s}\theta''_{s+1} + c_{1,s}\theta'_{s+1} + c_{2,s}f''_{s+1} + c_{3,s}f'_{s+1} + c_{4,s}f_{s+1} + c_{5,s}g'_{s+1} + c_{5,s}g_{s+1} = RHS3, \tag{23}$$

The parameters $a_{i,s}$, $b_{i,s}$, and $c_{i,s}$ (with i taking the values from $0, 1, 2, \cdots$) are required through prior calculations and are expressed as follows:

$$a_{0,s} = A_1 + K, a_{1,s} = -SqA_2\eta + SqA_2 f_s', a_{2,s} = -MA_3 - DaA_1 - 3SqA_2 - SqA_2 f_s',$$

$$a_{3,s} = -SqA_2 f_s'^{0'} + SqA_2 f_s''', a_{3,s} = -SqA_2 f_s^{''} + SqA_2 f_s^{'''}, a_{4,s} = K,$$

$$b_{0,s} = S_1\left(A_1 + \frac{K}{2}\right), b_{1,s} = -A_2 SqS_1\eta + SqA_2 S_1 f_s,$$

$$b_{2,s} = -2K - 3A_2 SqS_1 - A_2 SqS_1 f_s', b_{3,s} = -K, b_{4,s} = -SqA_2 S_1 g_s, b_{5,s} = A_2 SqS_1 g_s',$$

$$c_{0,s} = A_4 + Nr, c_{1,s} = -A_5 SqPr\eta + SqA_5 Prf_s, c_{2,s} = PrKEcf_s^{''} + 2f_s^{''}\frac{\Pr Ec}{A_1},$$

$$c_{3,s} = \frac{\Pr Ec}{A_1}8\delta^2 f_s' + 2f_s'\Pr EcMA_3, c_{4,s} = A_5 SqPr\theta_s' + 2f_s\delta^2\Pr EcMA_3,$$

$$c_{5,s} = \frac{\Pr EcS_1}{A_1}\left[1 + \frac{K}{2}(1-\phi)^{2.5}\right]2g_s',$$

$$c_{6,s} = K\Pr Ec4g_s + \frac{\Pr EcS_1}{A_1}\left[1 + \frac{K}{2}(1-\phi)^{2.5}\right]2\delta^2 g_s. \quad (24)$$

The right-hand side expressions of Eqs. (26) to (28) are defined as

$$RHS1 = -SqA_2 f_s^{'f_s''} + SqA_2 f_s^{'f_s'''},$$

$$RHS2 = -SqA_2 S_1 f_s' g_s + A_2 SqS_1 f_s g_s',$$

$$\begin{aligned} RHS3 = {} & A_5 Sq\Pr f_s\theta_s' + \frac{KPrEc}{2}\left(f_s''\right)^2 + K\Pr Ec2\left(g_r\right)^2 \\ & + \frac{PrEc}{A_1}4\delta^2\left(f_s'\right)^2 + \frac{PrEc}{A_1}\left(f_s''\right)^2 \\ & + \frac{PrEcS_1}{A_1}\left[1 + \frac{K}{2}(1-\phi)^{2.5}\right]\delta^2\left(g_s\right)^2 \\ & + \frac{PrEcS_1}{A_1}\left[1 + \frac{K}{2}(1-\phi)^{2.5}\right]\left(g_s'\right)^2 \\ & + \Pr EcMA_3\delta^2\left(f_s\right)^2 + \Pr EcMA_3\left(f_s'\right)^2. \end{aligned} \quad (25)$$

Utilizing the Chebyshev spectral collocation method, Eqs. (26) to (28) are solved for f_{s+1}, g_{s+1}, and θ_{s+1}. The process kicks off with an appropriate initial guess, specifically chosen as a function that satisfies the boundary conditions. The initial guesses are as follows:

$$f_0(\eta) = \frac{3}{2}\eta - \frac{\eta^3}{2}, g_0(\eta) = 0, \text{and} \theta_0(\eta) = \eta^2. \quad (26)$$

Initiating the solution process for Eqs. (26) to (28) involves discretizing these equations through the application of the Chebyshev spectral method within the interval $[-1, 1]$. To facilitate numerical computations, it is crucial to convert the domain $[0, 1]$ into a computational range of $[-1, 1]$. This conversion is achieved using the equation $\eta = (\xi + 1)/2$. Subsequently, a differentiation matrix D is introduced to estimate the unknown variables, $f(\eta)$, $g(\eta)$, and $\theta(\eta)$, at the collocation points using a matrix–vector product, as described below:

$$\left.\begin{array}{l} \frac{\partial f}{\partial \eta} = \sum_{k=0}^{N} D_{kj} f\left(\xi_k\right) = \boldsymbol{D}F, j = 0, 1, \ldots, N, \\ \frac{\partial g}{\partial \eta} = \sum_{k=0}^{N} D_{kj} g\left(\xi_k\right) = \boldsymbol{D}G, j = 0, 1, \ldots, N \\ \frac{\partial \theta}{\partial \eta} = \sum_{k=0}^{N} D_{kj} \theta\left(\xi_k\right) = \boldsymbol{D}\Theta, j = 0, 1, \ldots, N \end{array}\right\}, \quad (27)$$

where N is the number of collocation points, $D = 2D$,

$$f = \left[F\left(\xi_0\right), F\left(\xi_1\right), \ldots, F\left(\xi_N\right)\right]^T,$$
$$g = \left[G\left(\xi_0\right), G\left(\xi_1\right), \ldots, G\left(\xi_N\right)\right]^T, \text{and}$$
$$g\theta = \left[\Theta\left(\xi_0\right), \Theta\left(\xi_1\right), \ldots, \Theta\left(\xi_N\right)\right]^T.$$

Equations (26) to (28) can be expressed in matrix form as

$$\begin{bmatrix} A_{11} & A_{12} & A_{13} \\ A_{21} & A_{22} & A_{23} \\ A_{31} & A_{32} & A_{33} \end{bmatrix}\begin{bmatrix} f_{s+1} \\ g_{s+1} \\ \theta_{s+1} \end{bmatrix} = \begin{bmatrix} RHS1 \\ RHS2 \\ RHS3 \end{bmatrix}, \quad (28)$$

where

$$A_{11} = a_{0,s}\boldsymbol{D}^4 + diag\left[a_{1,s}\right]\boldsymbol{D}^3 + diag\left[a_{2,s}\right]\boldsymbol{D}^2 + diag\left[a_{3,s}\right]\boldsymbol{D}, A_{12} = a_{4,s}\boldsymbol{D}^2, A_{13} = 0,$$

$$A_{21} = b_{3,s}\boldsymbol{D}^2 + diag\left[b_{4,s}\right]\boldsymbol{D} + diag\left[b_{5,s}\right],$$

$$A_{22} = b_{0,s}\boldsymbol{D}^2 + diag\left[b_{1,s}\right]\boldsymbol{D} + diag\left[b_{2,s}\right], A_{23} = 0,$$

$$A_{31} = diag\left[c_{2,s}\right]\boldsymbol{D}^2 + diag\left[c_{3,s}\right]\boldsymbol{D} + diag\left[c_{4,s}\right], A_{32} = c_{0,s}\boldsymbol{D}^2 + diag\left[c_{1,s}\right]\boldsymbol{D}, A_{33} = 0.$$

where *diag* represents a diagonal matrix of size $(N + 1) \times (N + 1)$, I is an identity matrix of size $(N + 1) \times (N + 1)$, and D represents differentiation with respect to η.

5 Results and Discussion

The spectral quasilinearization method is employed for the efficient solution of the designed equations proposed in the current problem. To demonstrate the convergence of the SQLM numerical scheme, the errors are calculated up to a certain accuracy. These errors represent the disparities between the estimated function values at consecutive iterations. To illustrate the convergence of SQLM, infinity norms are utilized, which are defined as follows:

$$E_f = \max_{0\le s\le N} \|f_{s+1,x} - f_{s,x}\|_\infty, E_g = \max_{0\le s\le N} \|g_{s+1,x} - g_{s,x}\|_\infty, E_\theta = \max_{0\le s\le N} \|\theta_{s+1,x} - \theta_{s,x}\|_\infty.$$

Table 1 displays the solution errors of E_f, E_g, and E_θ, which were computed using the SQLM at various iteration levels. It is evident that the error norm decreases as the number of iterations increases for each of the functions. This observation indicates that the SQLM numerical method exhibits rapid convergence as the error consistently diminishes with an increasing number of iterations.

Once again, the precision of the SQLM by assessing the residual error norm at infinity for each function is verified. The determination of the infinity norm entails substituting the approximate solutions into the differential Eqs. (26)–(28). The norms are precisely defined as follows:

$$\|Res(f)\|_\infty = \|(A_1 + K) f_s^{iv} + K g_s'' - M A_3 f_s'' - Da A_1 f_s'' - Sq A_2 (3 f_s'' + \eta f_s''' + f_s' f_s'' - f_s' f_s''')\|_\infty,$$

$$\|Res(g)\|_\infty = \|S_1 \left(A_1 + \frac{K}{2}\right) g_s'' - K f_s'' - 2K g_s - A_2 Sq S_1 (3 g_s + \eta g_s' + f_s' g_s - f_s g_s')\|_\infty,$$

$$\|Res(\theta)\|_\infty = \|(A_4 + Nr)\theta_s'' - A_5 Sq Pr(\eta\theta_s' - f_s\theta_s') + \frac{KPrEc}{2}(f_s'' + 2g_s)^2 + \frac{PrEc}{A_1}(4 f_s'^2 \delta^2 + f_s''^2) + \frac{PrEcS_1}{A_1}\left[1 + \frac{K}{2}(1-\phi)^{2.5}\right](\delta^2 g_s^2 + g_s''^2) + PrEcMA_3(\delta^2 f_s^2 + f_s'^2)\|_\infty.$$

Table 2 illustrates the variation of the residual error with respect to the number of iterations. It is evident from the table that the residual error consistently decreases as the number of iterations increases. The decreasing norm of the residual indicates an improvement in the accuracy of the approximate solutions obtained using the SQLM. Moreover, the convergence is achieved as the norm of the residual decreases. The results presented in the table further affirm that the SQLM is a robust and accurate numerical method for effectively solving nonlinear differential equations.

However, the proposed methodology SQLM has certain limitations and these are generally the linearized approximation not accurately produce the behavior of the original nonlinear system, convergence procedure may require a large number of iterations, which will increase computational time and resource requirements, The quasilinearization method is sensitive to the choice of initial guess for the solution, etc.

6 Parametric Behavior

Squeezing the flow of blood-based micropolar hybrid nanofluid comprised of *Cu* and *Ag* is proposed in this article with the association of dissipation together with thermal radiation. The thermal attribute defining the density, specific heat,

Table 1 Convergence of the SQLM for $f(\eta)$, $g(\eta)$, and $\theta(\eta)$

Iterations	E_f	E_g	E_θ
1	6.585×10^{-3}	1.448×10^{-1}	1.016×10^{-1}
2	1.375×10^{-7}	1.040×10^{-6}	4.399×10^{-5}
3	3.536×10^{-13}	1.012×10^{-13}	2.980×10^{-10}
4	2.750×10^{-13}	1.946×10^{-13}	5.373×10^{-13}
5	3.050×10^{-13}	1.164×10^{-13}	4.508×10^{-13}
6	1.598×10^{-13}	1.439×10^{-13}	5.196×10^{-13}
7	3.525×10^{-13}	1.790×10^{-13}	1.931×10^{-14}
8	3.233×10^{-13}	1.776×10^{-13}	3.719×10^{-14}
9	2.219×10^{-13}	1.036×10^{-13}	1.676×10^{-14}
10	3.955×10^{-13}	2.747×10^{-13}	9.504×10^{-14}

Table 2 Residual error for Eqs. (26)–(28) obtained with the SQLM scheme

Iterations	$\|Res(f)\|_\infty$	$\|Res(g)\|_\infty$	$\|Res(\theta)\|_\infty$
1	1.260×10^{-4}	1.891×10^{-4}	5.549×10^{-3}
2	1.858×10^{-6}	3.023×10^{-5}	3.411×10^{-5}
3	2.994×10^{-8}	4.772×10^{-13}	2.094×10^{-12}
4	3.120×10^{-11}	2.273×10^{-13}	5.535×10^{-12}
5	2.479×10^{-11}	1.259×10^{-13}	5.622×10^{-12}
6	2.580×10^{-11}	4.700×10^{-13}	1.779×10^{-12}
7	1.886×10^{-11}	2.006×10^{-13}	7.955×10^{-12}
8	2.929×10^{-11}	3.987×10^{-13}	4.683×10^{-12}
9	2.256×10^{-11}	4.346×10^{-13}	1.448×10^{-12}
10	3.979×10^{-11}	5.611×10^{-13}	4.166×10^{-12}

Table 3 Thermal attributes of the solid particles and blood

	$\rho(Kg/m^3)$	$c_p(J/KgK)$	$k(Wm^{-1}K^{-1})$	$\sigma(S/m)$
Copper(*Cu*)	8933	385	400	5.96×10^7
Silver(*Ag*)	10,500	235	429	3.6×10^7
Blood	1063	3549	0.492	4.3×10^{-5}

Table 4 Comparison of the values of $-\theta'(1)$ with previously published work of Ref. [32], Ref. [34], and Ref. [35] for different values of Sq when $Ec = Pr = 1$

Sq	Mustafa et al. [32]	Gupta and Ray [34]	Kumar et al. [35]	Present
−1.0	3.319899	3.31989925	3.31991041	3.3199
−0.5	3.129491	3.12949109	3.12949100	3.1295
0.01	3.047092	3.04709193	3.04709268	3.0471
0.5	3.026324	3.02632345	3.02635546	3.0264
2.0	3.118551	3.11854353	3.11890544	3.1189

Table 5 Comparison of the values of $f''(1)$ with previously published work of Ref. [32], Ref. [34], and Ref. [35] for different values of Sq when $Ec = Pr = 1$

Sq	Mustafa et al. [32]	Gupta and Ray [34]	Kumar et al. [35]	Present
−1.0	2.170090	2.17009087	2.1701501	2.1702
−0.5	2.614038	2.61740384	2.6174213	2.6174
0.01	3.007134	3.00713375	3.0071335	3.0071
0.5	3.336449	3.33644946	3.3364442	3.3364
2.0	4.167389	4.16738921	4.1674011	4.1674

thermal, as well as electrical conductivity of the nanoparticles, and the base liquids are depicted in Table 3. The coupled nonlinear form of the governing equations is solved through SQLM combined with the characterizing parameters defined within their standard range. The behavior of these parameters is depicted through graphs, and the numerical values for the shear and thermal transportation rates are presented in tabular form. Tables 4 and 5 show the validation of the present outcome of the rate of heat transportation and shear rate with the works of Mustafa et al. [32], Gupta and Ray [34], and Kumar et al. [35], considering various squeezing constraints. The result reveals a good correlation since both the results coincide with each other up to a certain accuracy which suggest the convergence criteria of the present methodology. The convergence of the methodology is presented briefly in the previous section.

The illustration of the magnetic parameter affecting the axial fluid velocity is depicted through Fig. 2. The comparative analysis is presented for the variation of $Ag \sim$ blood nanofluid (dotted) and $Ag + Cu \sim$ blood (solid) hybrid nanofluid. To discuss the physical behavior of the magnetic constraint

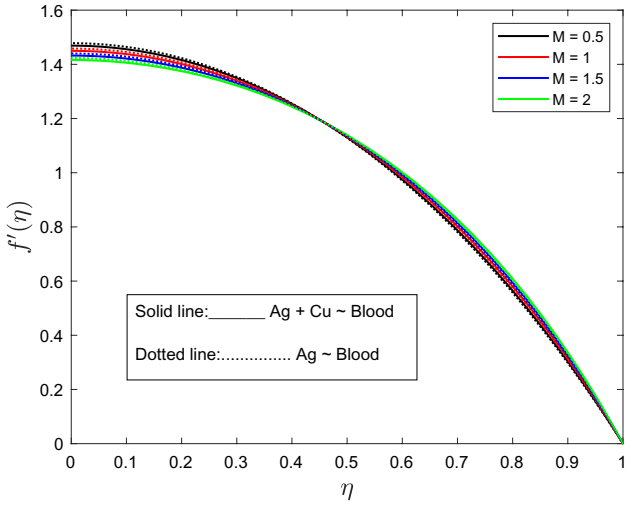

Fig. 2 $f'(\eta)$ versus η for different M

on the momentum profile, the range of the parameter is restricted to the standard numerical values of $0.5 \leq M \leq 2$. The applied magnetic field proposed toward the normal direction of the fluid velocity urges to produce an external force, i.e., treated as a resistive force known to be "Lorentz force" which has the ability to resists the fluid motion. Therefore, near the lower wall of the channel, the velocity profile retards with the upsurging magnetization, and further, it reveals a dual characteristic from the point of inflection. It is seen that the momentum profile enhances toward the upper wall of the channel from central region. It validates the fact of the restive force produced by the magnetic property. Moreover, the characteristic of the solid nanoparticles reveals that the hybrid nanofluid attenuates the velocity profile which is more pronounced than the nanofluid. The fact is because of the heavier density of the nanoparticles and the combined effect both the solid particles. Figure 3 portrays the characteristic of the magnetic parameter on the temperature profile when both the scenario of nanofluid and hybrid nanofluid is presented. The stored energy near the lower wall of the channel led to boosting up the profile, and the fluid temperature rises significantly with the growing magnetic parameter. The importance of the enhanced profile is due to the effective thermophysical properties used in the energy distribution. One of the important factors in the entire distribution is the use of the particle concentration since the addition of particle concentration carrying out the behavior of all the physical models is considered. Figure 4 shows the role of the solid particle volume concentration affecting the axial velocity profile. Here, the range of the volume fraction is considered $0.01 \leq \phi \leq 0.08$ where both the behavior of *Ag* and *Cu* nanoparticles is presented briefly. Particle concentration is the dispersion of nanoparticles into the base fluid. In the first case, the solid silver particles are dispersed into the blood to prepare nanofluid, and

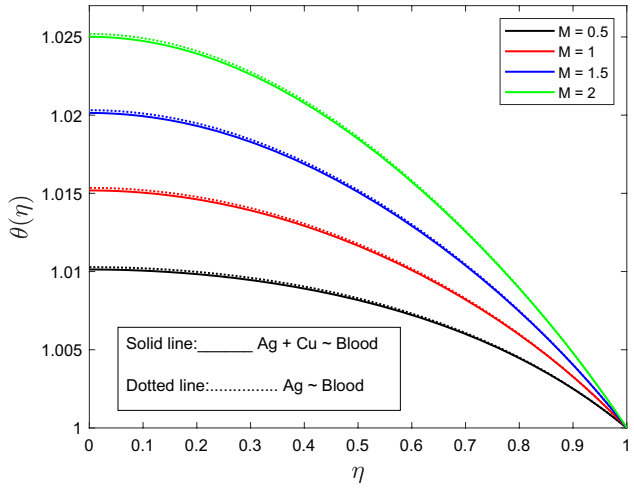

Fig. 3 $\theta(\eta)$ versus η for different M

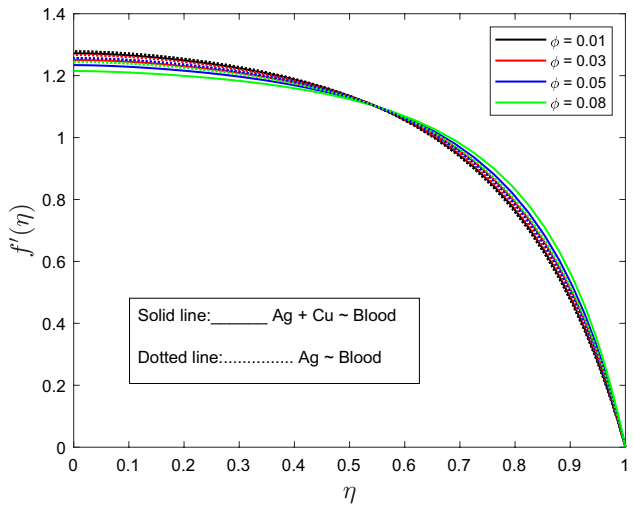

Fig. 4 $f'(\eta)$ versus η for different ϕ

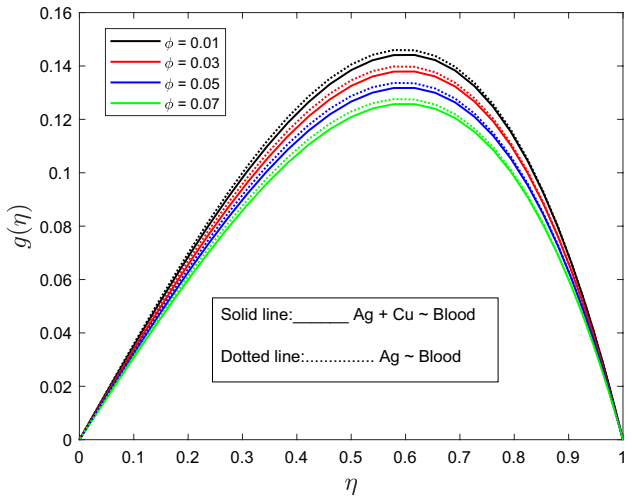

Fig. 5 $g(\eta)$ versus η for different ϕ

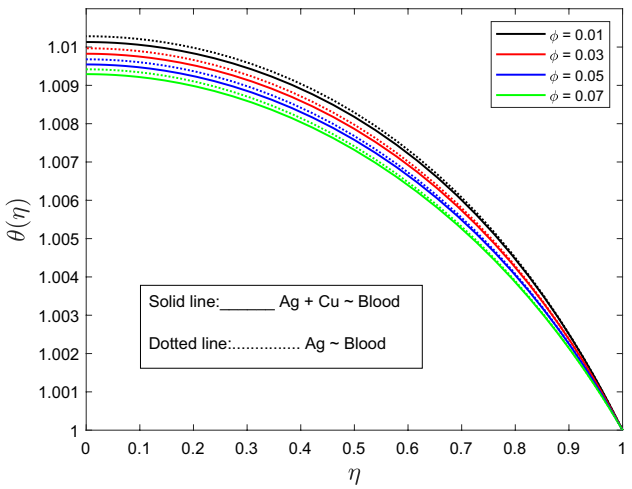

Fig. 6 $\theta(\eta)$ versus η for different ϕ

further, copper nanoparticles are dispersed in to the nanofluid to observe the behavior of hybrid nanofluid. The greater density of the nanofluid as well as hybrid nanofluid decelerates the velocity profile. This deceleration is projected smoothly near the lower wall up to the center of the channel, and afterward, reverse impact is rendered as the domain increases. A sharp fall in the profile is marked toward the upper wall of the channel. Therefore, it is noteworthy to conclude that it is beneficial to use the concentrated fluid which is favorable in restricting the velocity within the channel. Figure 5 demonstrates the impact of the particle concentration on the angular velocity with the variation of nanofluid and hybrid nanofluid. The profile became symmetric about the center of the channel irrespective to the type of fluid considered. The result reveals that with the increasing concentration, the profile thickness diminishes at both the channel walls. However, the strength of the hybrid nanofluid is dominated by the nanofluid significantly within the domain. Figure 6 explores the effect of particle concentration of the nanoparticles on the fluid temperature distribution. As discussed above, the effectiveness of the fluid properties exhibited due to the factor of concentration and the conductivity of the nanofluid as well as the hybrid nanofluid energies the properties in comparison to the conventional fluid. Therefore, the energy at the upper wall of the channel will flows toward the lower wall with the increasing concentration and the fluid temperature upsurges in magnitude. The case of hybrid nanofluid attenuates the thickness at the lower wall as compared to the upper wall. Figure 7 exhibits the role of the squeezing constant on the axial velocity profile of the micropolar fluid. The characteristic is displayed for both the case of nanofluid and hybrid nanofluid. The discussion is presented for the adaptation of the particular

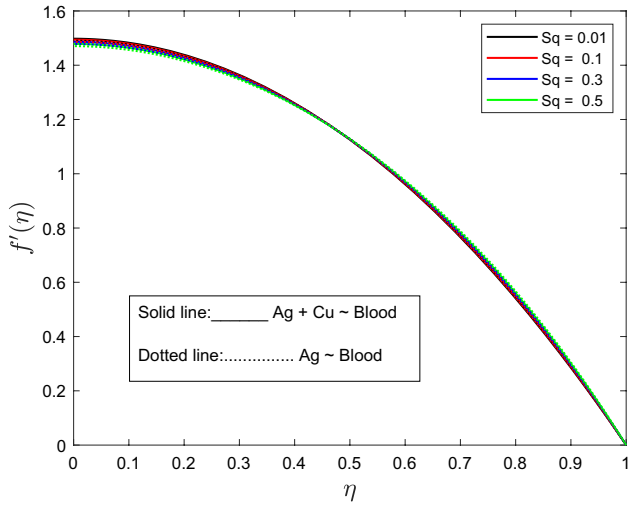

Fig. 7 $f'(\eta)$ versus η for different Sq

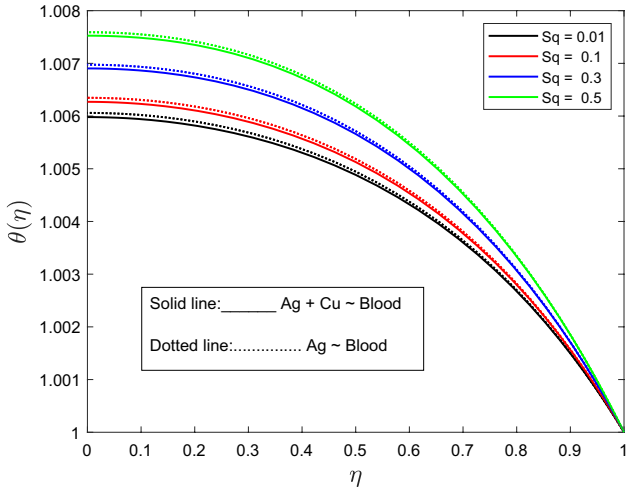

Fig. 9 $\theta(\eta)$ versus η for different Sq

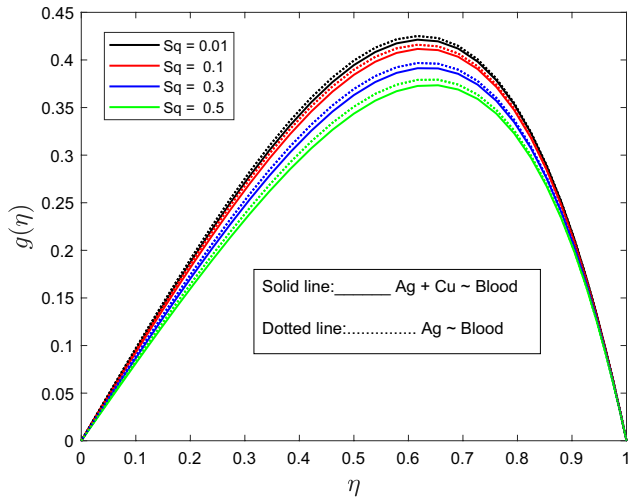

Fig. 8 $g(\eta)$ versus η for different Sq

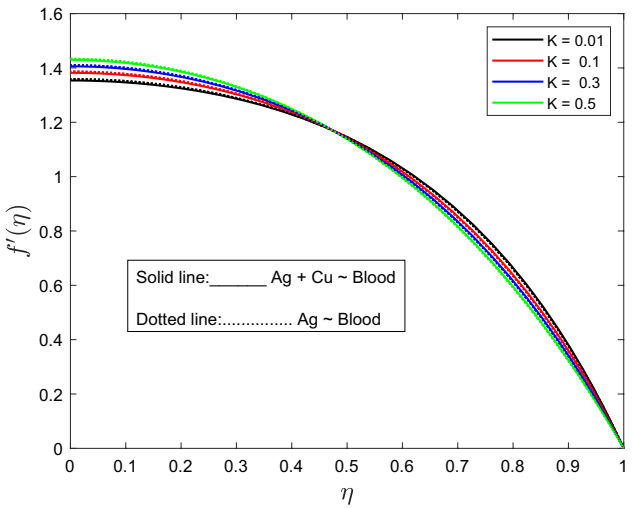

Fig. 10 $f'(\eta)$ versus η for different K

constraint within the range $0.01 \leq Sq \leq 0.5$. First of all, the positive values of the parameter suggest that both the walls move away from each other and the increasing range is dedicated to the increasing distance between the walls. The dual characteristic is obtained in the fluid velocity distribution from the central region of the channel. It is seen that the lower wall and the upper wall thickness reduces for the increasing squeezing parameter. Figure 8 characterizes the physical behavior of the squeezing constant on the angular momentum profile. One of the interesting facts is that the profile became tilled toward the upper wall region and its strength retards from both the wall region. Figure 9 displays the variation of squeezing parameter affecting the fluid temperature where the variation is depicted for both the scenario of nanofluid and hybrid nanofluid. As the difference between the walls increases, the fluid temperature leads to enhance the temperature of the fluid and this enrichment is greater in the situation of nanofluid in comparison to the hybrid nanofluid near to the lower wall. However, the growing domain of the profile attenuates significantly to meet adequate boundary constraints. Figure 10 renders the physical significance of the non-Newtonian constraint that is presented in the form of micropolar parameter on the fluid velocity. The micropolar parameter which is mathematically presented as $K = \kappa/\mu$ varies within a standard value of $0.01 \leq K \leq 0.5$. Physically, the higher values of the material parameter signify the lesser in fluid viscosity. Therefore, the less viscous fluid has greater velocity which validates the fact presented here. Further, the existence of rotational viscosity that creates the non-Newtonian feature of the fluid conforms greater in fluid velocity

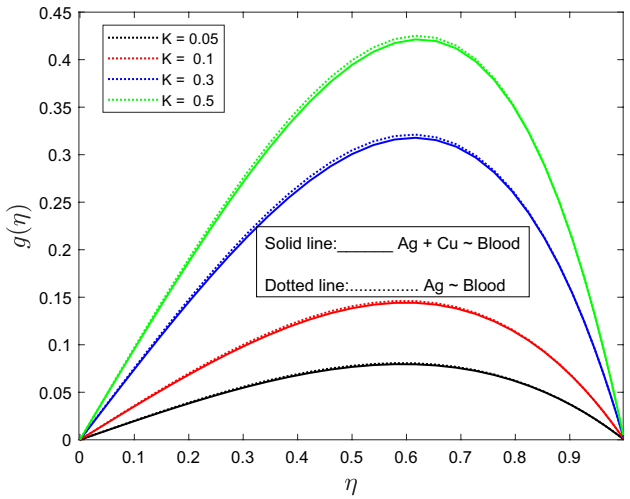

Fig. 11 $g(\eta)$ versus η for different K

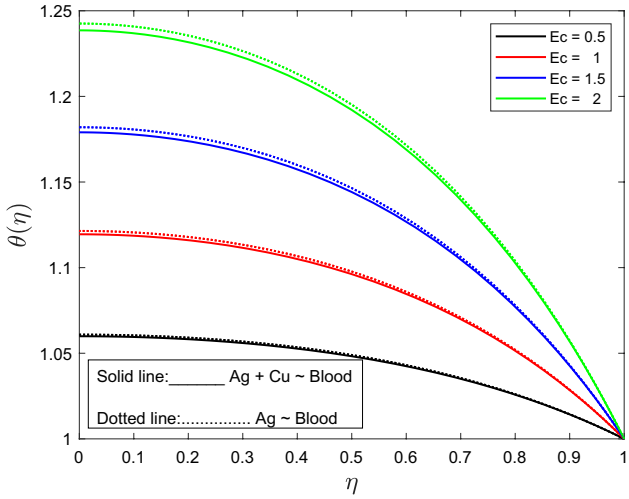

Fig. 13 $\theta(\eta)$ versus η for different Ec

irrespective to the type of fluid considered. Further, the comparative analysis shows a two-fold form of the profile deviating from the central region of the channel. Near the lower wall, it is seen that the profiles of nanofluid dominate the fact of hybrid nanofluid, but the impact is opposite when domain varies from the center to the upper wall. Figure 11 portrays the characteristic of the factor relating to the micropolar parameter on the transverse velocity distribution. The significant behavior is depicted for the variation of $Ag\sim$blood and $Ag+Cu\sim$blood hybrid nanofluid with the existence of other parameters. The profiles became symmetric with respect to center region, and it shows that its maximum magnitude arises at the center from where the profile falls toward the wall region. Further, the enhanced material parameter augments the profile strength toward both the walls. Moreover, the strength of the $Ag\sim$blood nanofluid dominates the case of blood-based hybrid nanofluid. Figure 12 depicts the role of thermal radiation on the fluid temperature with the variation of various types of nanofluids. Thermal radiation is generally used as a measure of the emitted electromagnetic waves from the surface of the fluid element. Further, this electromagnetic wave is transformed to thermal radiation. Therefore, the enhanced thermal radiation is supposed to improve the heat transport phenomenon, and this causes the increasing fluid temperature. Again, the hybrid nanofluid has a dominating characteristic over the case of nanofluid within the proposed domain. Figure 13 illustrates the significant role of the coupling constant affecting the fluid temperature. The non-dimensional constraint Ec is obtained due to the inclusion of the dissipative heat which makes the set of governing

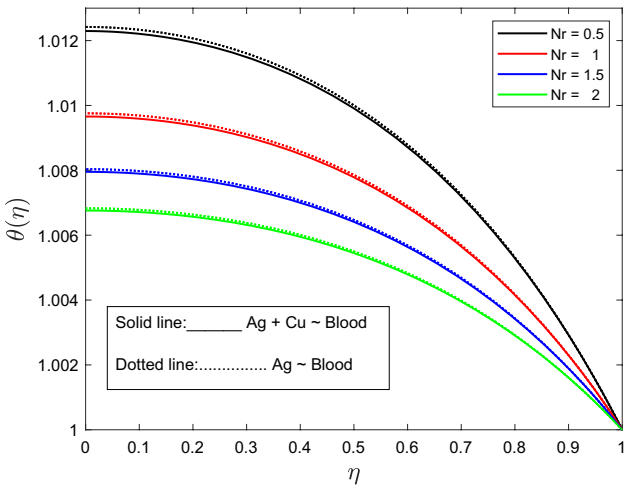

Fig. 12 $\theta(\eta)$ versus η for different Nr

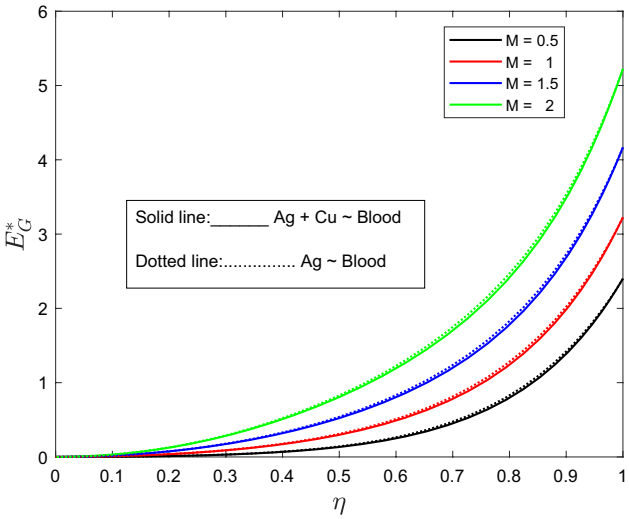

Fig. 14 $E_G{}^*$ versus η for different M

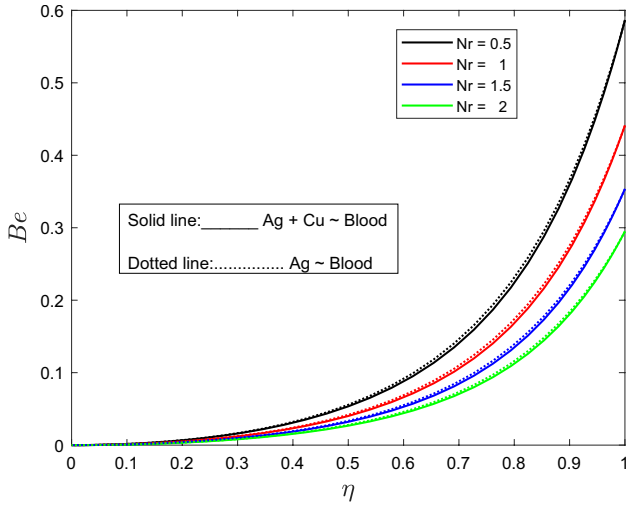

Fig. 15 *Be* versus η for different *Nr*

equation coupled. Mathematically, *Ec* is defined as the change in enthalpy of the kinematic viscosity. The increasing Eckert number signifies the reduction in enthalpy and this provides a significant hike in the fluid temperature at the lower wall. The boosted temperature distribution is due to the effective thermal properties adopted for the nanofluid.

The computation of the heat transport phenomenon along with the flow profiles and the irreversibility process within the system is presented by the computation of the entropy analysis. Generally, irreversibility occurs due to several processes, i.e., irreversibility due to heat transfer, due to dissipation, and due to diffusion processes, respectively. Further, the computation of the Bejan number is depicted which is obtained by the ratio between the irreversibility due to heat transfer and total entropy. Figure 14 describes the impact of magnetization on the entropy generation. The interaction of magnetic parameter and entropy generation is essential in different scientific and technological applications including information storage technologies, advanced cooling system, etc. With the increasing domain, the entropy change is drastic. There is a significant hike in entropy for the enhanced magnetization. Further, the hybrid nanofluid is favorable in reducing velocity in comparison to the case of nanofluid. Figure 15 depicts the behavior of magnetic parameter on the value of the Bejan number. A similar tendency is rendered for the profile of the Bejan number with the variation of magnetization. Further, Fig. 16 explores the significant behavior of the thermal radiation on the Bejan value. It is seen that although the profile hikes are irrespective to the situation of nanofluid as well as hybrid nanofluid, the increasing radiation favors in controlling the heat transport properties.

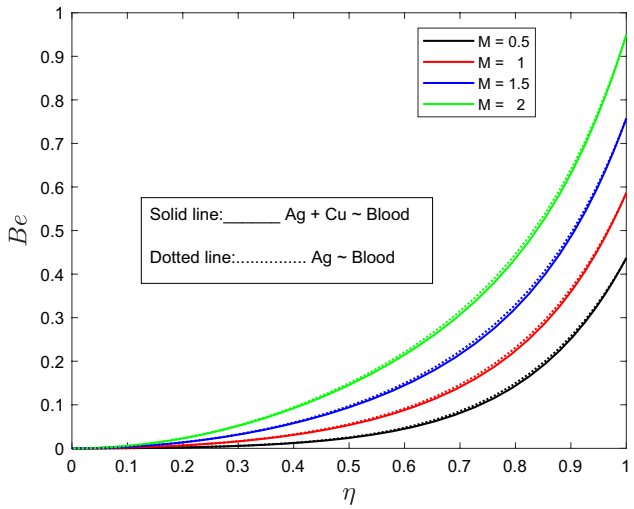

Fig. 16 *Be* versus η for different *M*

7 Conclusion

Entropy analysis on the squeezing flow of hybrid nanofluid in association with the blood-based *Ag* and *Cu* nanoparticles through a parallel channel is presented in this article. The dissipative heat along with the thermal radiation on the heat transport phenomena energizes the flow properties. The novelty of the proposed study is the solution of the governing equations using the spectral quasilinearization method and the comparative analysis with the work of others' investigations. The important conclusive remarks are as follows:

- The validation and the comparative analysis with the earlier work suggest a good correlation and present a suggestive measure to carry out the research.
- The fluid velocity shows its dual properties within the domain irrespective to the type of fluid, but up to the central region, the profile of the fluid velocity enhances and afterward, the effect is reversed.
- Dissipative heat impact on the fluid temperature distribution is relevant, and the enhanced in Eckert number enhances the fluid temperature.
- Entropy analysis due to various factors favors in successive growth of profiles of entropy and the Bejan number.

Further, the proposed study neither describes the parametric contribution on the various profiles but also gives synergetic impact in several applications used in daily life. Other than high cooling efficiency of the hybrid nanofluid, the present study is useful in production processes in industries and biomedical applications like blood pumping, drug delivery, cancer treatment, etc.

Author Contribution All authors have equally contributed to complete the manuscript, i.e., TA has formulated the problem and verified the problem statement; RB has completed the introduction section; SRM has computed and simulated the numerical results, and finally, SP checked the correctness of grammar and the results and discussion section and checked the overall data.

Funding None.

Data Availability No datasets were generated or analyzed during the current study.

Code Availability Not applicable.

Declarations

Ethics Approval The entire work is the original work of the authors.

Consent to Participate Not applicable.

Consent for Publication All the authors have given their consent to publish the paper.

Conflict of Interest None.

Research Involving Humans and Animals Statement None.

Informed Consent None.

References

1. Sarwar, N., Asjad, M. I., Hussain, S., Alam, Md. N., & Inc, M. (2022). Inclined magnetic field and variable viscosity effects on bioconvection of Casson nanofluid slip flow over non linearly stretching sheet. *Propulsion and Power Research, 11*(4), 565–574. https://doi.org/10.1016/j.jppr.2022.09.002
2. Lone, S. A., Raizah, Z., Shah, M. H., Rehman, S., Saeed, A., & Eldin, S. M. (2023). Thermal and Solutal slips impact on 3D-convection flow of linearly stratified Casson nanofluid (magnesium-blood) passed over a bi-stretching surface in a rotating frame. *Results in Physics, 55*, 107139. https://doi.org/10.1016/j.rinp.2023.107139
3. Baithalu, R., Mishra, S. R., Pattnaik, P. K., & Panda, S. (2023). Optimizing shear and couple stress analysis for the magneto-micropolar dissipative nanofluid flow toward an elongating surface: A comprehensive RSM-ANOVA investigation. *Journal of Thermal Analysis and Calorimetry*. https://doi.org/10.1007/s10973-023-12741-w
4. Farooq, U., Waqas, H., Alhazmi, E. S., Alhushaybari, A., Imran, M., Sadat, R., Muhammad, T., & Ali, M. R. (2023). Numerical treatment of Casson nanofluid bioconvectional flow with heat transfer due to stretching cylinder/plate: Variable physical properties. *Arabian Journal of Chemistry, 16*(4), 104589. https://doi.org/10.1016/j.arabjc.2023.104589
5. Mishra, S. R., Pattnaik, P. K., Ontela, S., & Panda, S. (2023). Characterization of shape factor with multi slip and inclined magnetized radiative Casson hybrid nanofluid transport in an expanding/contracting convective sheet. *Partial Differential Equations in Applied Mathematics, 8*, 100570. https://doi.org/10.1016/j.padiff.2023.100570
6. Panda, S., Pradhan, G., Nayak, D., Pattnaik, P. K., & Mishra, S. R. (2023). Presentation of entropy due to heat transfer irreversibility of MHD Williamson fluid over an inclined channel. *Modern Physics Letters B*, *38*(07). https://doi.org/10.1142/s0217984924500106.
7. Shao, W., Baithalu, R., Mishra, S. R., Dogonchi, A. S., Ali, R., Chamkha, A. J., & Galal, A. M. (2024). Statistical approach on optimizing heat transfer rate for au/FE3O4-blood nanofluid flow with entropy analysis used in drug delivery system. *Case Studies in Thermal Engineering*, 104008. https://doi.org/10.1016/j.csite.2024.104008.
8. Panda, S., Thumma, T., Ontela, S., Mishra, S. R., & Pattnaik, P. K. (2023). A numerical study on model-based comparative analysis for MHD magnetite (fe3o4) and cobalt ferrite (COFE2O4) flow past a heated shrinking Riga surface with radiative heat flux. *Journal of Magnetism and Magnetic Materials, 586*, 171212. https://doi.org/10.1016/j.jmmm.2023.171212
9. Azam, M., Xu, T., Mabood, F., & Khan, M. (2021). Non-linear radiative bioconvection flow of cross nano-material with gyrotatic microorganisms and activation energy. *International Communications in Heat and Mass Transfer, 127*, 105530. https://doi.org/10.1016/j.icheatmasstransfer.2021.105530
10. Khan, M. I., & Alzahrani, F. (2021). Dynamics of viscoelastic fluid conveying nanoparticles over a wedge when bioconvection and melting process are significant. *International Communications in Heat and Mass Transfer, 128*, 105604. https://doi.org/10.1016/j.icheatmasstransfer.2021.105604
11. Habib, U., Abdal, S., Siddique, I., & Ali, R. (2021). A comparative study on micropolar, Williamson, Maxwell nanofluids flow due to a stretching surface in the presence of bioconvection, double diffusion and activation energy. *International Communications in Heat and Mass Transfer, 127*, 105551. https://doi.org/10.1016/j.icheatmasstransfer.2021.105551
12. Waqas, H., Farooq, U., Muhammad, T., Hussain, S., & Khan, I. (2021). Thermal effect on bioconvection flow of Sutterby nanofluid between two rotating disks with motile microorganisms. *Case Studies in Thermal Engineering, 26*, 101136. https://doi.org/10.1016/j.csite.2021.101136
13. Nayak, B., Acharya, S., & Mishra, S. R. (2022). Impact of dissipative heat and thermal radiation on the steady magnetohydrodynamic nanofluid flow with an interaction of Brownian motion and chemical reaction. *International Journal of Applied and Computational Mathematics*, *8*(3). https://doi.org/10.1007/s40819-022-01345-x.
14. Lone, S. A., Raizah, Z., Shah, M. H., Rehman, S., Saeed, A., & Eldin, S. M. (2023). Thermal and Solutal slips impact on 3D-biconvection flow of linearly stratified Casson nanofluid (magnesium-blood) passed over a bi-stretching surface in a rotating frame. *Results in Physics, 55*, 107139. https://doi.org/10.1016/j.rinp.2023.107139
15. Saleem, S., Abbas, T., Abutuqayqah, H., UlHaq, E., & Ullah Khan, S. (2023). Numerical simulation accompanied by an intelligent computing system for the chemical reaction of Casson nanofluid and radiative heat flux on a nonlinear stretching surface. *Alexandria Engineering Journal, 79*, 629–643. https://doi.org/10.1016/j.aej.2023.08.016
16. Raut, P., & Mishra, S. R. (2023). Diversified impact of carbon nanotubes on the flow of micropolar nanofluid over a permeable expanding/contracting surface with thermal radiation. *Modern Physics Letters B*, *38*(08). https://doi.org/10.1142/s0217984924500490.
17. Hayat, T., Khan, M. I., Qayyum, S., & Alsaedi, A. (2018). Entropy generation in flow with silver and copper nanoparticles. *Colloids and Surfaces A: Physicochemical and Engineering Aspects, 539*, 335–346. https://doi.org/10.1016/j.colsurfa.2017.12.021
18. Iqbal, M., Khan, N. S., Khan, W., Hassine, S. B., Alhabeeb, S. A., & Khalifa, H. A. (2024). Partially ionized bioconvection Eyring-Powell nanofluid flow with gyrotactic microorganisms in thermal system. *Thermal Science and Engineering Progress, 47*, 102283. https://doi.org/10.1016/j.tsep.2023.102283

19. Mukdasai, K., & Nazir, U. (2023). Galerkin scheme on entropy generation in complex fluid involving gyrotactic microorganisms on cylinder/surface via solar thermal radiations. *Case Studies in Thermal Engineering, 45*, 102995. https://doi.org/10.1016/j.csite.2023.102995
20. Fatima, N., Belhadj, W., Nisar, K. S., Usman, Alaoui, M. K., Arain, M. B., & Ijaz, N. (2023). Heat and mass transmission in a boundary layer flow due to swimming of motile gyrotactic microorganisms with variable wall temperature over a flat plate. *Case Studies in Thermal Engineering, 45*, 102953. https://doi.org/10.1016/j.csite.2023.102953
21. Yusuf, T. A. (2023). Entropy analysis of unsteady MHD nanofluid flow over a stretching surface with effects of variable viscosity and nonuniform heat generation. *Numerical Heat Transfer, Part A: Applications*, 1–18.
22. Yusuf, T. A. (2023). Analysis of entropy generation in nonlinear convection flow of unsteady magneto-nanofluid configured by vertical stretching sheet with Ohmic heating. *International Journal of Ambient Energy, 44*(1), 2319–2335.
23. Yusuf, T. A., Ukaegbu, J. C., & Ayinde, A. M. (2022). Irreversibility analysis in the hydrothermal flow of γ Al2O3/H2O and γ Al2O3/C2H6O2 over a permeable stretching surface with effective Prandtl number. *Waves in Random and Complex Media*, 1–21.
24. Yusuf, T. A., Adesanya, S. O., & Gbadeyan, J. A. (2020). Entropy generation in MHD Williamson nanofluid over a convectively heated stretching plate with chemical reaction. *Heat Transfer, 49*(4), 1982–1999.
25. Yusuf, T. A., Mabood, F., Khan, W. A., & Gbadeyan, J. A. (2020). Irreversibility analysis of Cu-TiO2-H2O hybrid-nanofluid impinging on a 3-D stretching sheet in a porous medium with nonlinear radiation: Darcy-Forchhiemer's model. *Alexandria Engineering Journal, 59*(6), 5247–5261.
26. Khan, W. A., Yusuf, T. A., Mabood, F., Siddiq, M. K., & Shehzad, S. A. (2023). Chemically reactive water-based carbon nanotubes flow saturated in Darcy-Forchheimer porous media coupled with entropy generation. *Chemical Physics Letters, 830*, 140808.
27. Ahmed, S., Chen, Z. M., Xu, H., & Ishaq, M. (2024). Mixed convection flow in a square lid-driven cavity subject to inclined magnetic field with highly accurate wavelet-homotopy solutions. *Computers & Mathematics with Applications, 162*, 33–51.
28. Ahmed, S., Chen, Z. M., & Ishaq, M. (2023). Multiple solutions in magnetohydrodynamic stagnation flow of hybrid nanofluid past a sheet with mathematical chemical reactions model and stability analysis. Physics of Fluids, 35(7).
29. Ahmed, S., Xu, H., Zhou, Y., & Yu, Q. (2022). Modelling convective transport of hybrid nanofluid in a lid driven square cavity with consideration of Brownian diffusion and thermophoresis. *International Communications in Heat and Mass Transfer, 137*, 106226.
30. Ahmed, S., Xu, H., & Sun, Q. (2023). Coiflet wavelet-homotopy solutions to bio-thermal convection in a square cavity. *Advances in Applied Mathematics and Mechanics, 15*(3), 684–718.
31. Ahmed, S., & Xu, H. (2021). Forced convection with unsteady pulsating flow of a hybrid nanofluid in a microchannel in the presence of EDL, magnetic and thermal radiation effects. *International Communications in Heat and Mass Transfer, 120*, 105042.
32. Mustafa, M., Hayat, T., & Obaidat, S. (2012). On heat and mass transfer in the unsteady squeezing flow between parallel plates. *Meccanica, 47*, 1581–1589.
33 Motsa, S. S. (2013). A new spectral local linearization method for nonlinear boundary layer flow problems. *Journal of Applied mathematics, 2013*, 423628. https://doi.org/10.1155/2013/423628
34. Gupta, A. K., & Ray, S. S. (2015). Numerical treatment for investigation of squeezing unsteady nanofluid flow between two parallel plates. *Powder Technology, 279*, 282–289.
35. Kumar, N. N., Sastry, D. R. V. S. R. K., & Shaw, S. (2022). Irreversibility analysis of an unsteady micropolar CNT-blood nanofluid flow through a squeezing channel with activation energy-Application in drug delivery. *Computer Methods and Programs in Biomedicine, 226*, 107156.

Publisher's Note Springer Nature remains neutral with regard to jurisdictional claims in published maps and institutional affiliations.

Springer Nature or its licensor (e.g. a society or other partner) holds exclusive rights to this article under a publishing agreement with the author(s) or other rightsholder(s); author self-archiving of the accepted manuscript version of this article is solely governed by the terms of such publishing agreement and applicable law.